*Y. M. Yao, P. Joo, S. C. Jana**

Department of Polymer Engineering, The University of Akron, Akron, OH, USA

A Surfactant-Free Microfluidic Process for Fabrication of Multi-Hollow Polyimide Aerogel Particles

This work focuses on fabrication of multi-hollow polyimide gel and aerogel particles from a surfactant-free oil-in-oil emulsion system using a microfluidic droplet generator operating under dripping mode. The multi-hollow gel and aerogel particles have strong potential in thermal insulation. Under jetting and tip-streaming regime of microfluidic flows, droplets are generated with no occluded liquid phase. The present study investigates a means of designing polyimide gel particles with plurality of internal liquid droplets by strategically manipulating the flow rates of the continuous and dispersed phase liquids through the microfluidic droplet generator. The multi-hollow polyimide aerogel particles obtained after supercritical drying of the gel particles present mesopores, high BET surface area, and excellent prospect for thermal insulation.

1 Introduction

Aerogels are well-known for their high porosity (often over 90 %), low bulk density, high surface area, excellent thermal stability, and low thermal conductivity (Jones, 2006; Nguyen et al., 2017). Thermally stable polyimide aerogels have been fabricated in different shapes such as cylinders (Kim et al., 2016), spherical microparticles (Kwon et al., 2014; Teo and Jana, 2019), core-shell microparticles (Teo et al., 2020), films (Guo et al., 2012; Saadatnia et al., 2019), and 3-D printed complex structures (Teo et al., 2019).

A factor in large-scale production of polyimide aerogels is the cost of the process and the price of chemicals. A two-step method is commonly used in synthesis of polyimides (Edwards and Maxwell, 1955). In the first step, linear chain polyamic acids usually with dianhydride endcaps are obtained by reacting a dianhydride and a diamine. The polyamic acid is reacted in the second step with polyamine crosslinkers, namely, tris(2-aminoethyl)amine (Teo and Jana, 2018), 1,3,5-triaminophenoxybenzene (Meador et al., 2012), or octa(aminophenyl)-silsesquioxane (Guo et al., 2011) and imidized chemically at room temperature using acetic anhydride and pyridine. The above crosslinkers are expensive. Recently Meador et al. (2015) synthesized polyimides using a commercially available crosslinker, 1,3,5-benzenetricarbonyl trichloride (BTC), that also provided faster crosslinking reactions. In this work, the two-step chemistry presented above was followed for fabrication of nearly spherical polyimide gel particles using a microfluidic droplet generation scheme. These particles had diameter close to a millimeter with multiple internal voids of diameter in the range of 100 to 500 micrometer.

Previous studies on aerogel microparticles, i. e., particles with diameter of a few hundred micrometer, expanded the applications of aerogels in drug delivery (Alnaief and Smirnova, 2010) and thermal insulation (Sabri et al., 2013). Emulsion formation by mechanical means is a common process to produce microparticles such as via water/oil (W/O) emulsion (Alnaief and Smirnova, 2011) or oil/oil (O/O) emulsion (Gu et al., 2016). One can form surfactant-stabilized emulsions by hydrodynamically mixing two immiscible liquids via mechanical stirring, such as Gu et al. (2016). However, the lack of control of microparticle size distribution, the stability of the process, and the use of large proportions of the continuous phase liquid and its associated recovery process do not meet the standard required for large-scale production. In view of this, investigators take advantage of the microfluidic devices to produce microparticles in a stable and controllable way with the help of UV-curable material or surfactant. Moreover, the mass ratio of dispersed and continuous phase liquids can be close to unity.

Dendukuri and Doyle (2009) used T-junction devices to obtain nonspherical microparticles steadily through lithography technique. Marquis et al. (2015) used flow-focusing device to generate Janus microparticles from sodium alginate and citrus pectin continuously through the use of a surfactant. Teo and Jana (2019) succeeded in making use of the coaxial microfluidic flow to fabricate surfactant-free polyimide aerogel microparticles via oil-in-oil emulsion. Teo et al. (2020) then extended the use of coaxial microfluidic flow in fabrication of core-shell aerogel microparticles via an oil-in-oil-in-oil emulsion.

Meanwhile, creating hollow spherical microparticles especially from aerogel precursors has become interesting as hollow microparticles possess higher specific surface area, higher

* Mail address: Sadhan C. Jana, Department of Polymer Engineering, The University of Akron, 250 South Forge Street, Akron, OH 44325-0301, USA
E-mail: janas@uakron.edu

IPP_IPP3989 – 10.9.20/reemers

porosity, an occluded micrometer size space at the center of the microparticles, and relatively lower thermal conductivity compared to non-hollow microparticles, but the fabrication process is complicated for large-scale production purposes. Schematic of several types of multi-hollow aerogel particles is presented in Fig. 1. Okushima et al. (2004) first presented a two-step method in T-injection device to obtain multi-hollow microparticles through double emulsions. Wang et al. (2014) used multiple transition tubes in co-axial geometry to create multi-hollow microparticles through double or triple emulsions. Later, Chen et al. (2008) took advantage of the compound-fluidic electrospray technique to obtain multi-hollow microcapsules using just one step, although the use of an external force from the electric field impose additional energy cost. Teo et al. (2020) used two T-junction droplet generators in succession each operating in jetting regime for fabrication of core-shell polyimide aerogel microparticles.

In this work, a much simpler method of fabrication of multi-hollow polyimide aerogel particles was developed that is not reliant on surfactants or an external field. The objective was to use an easy to fabricate and implement continuous flow process for manufacturing of multi-hollow polyimide aerogel particles from a single emulsion. The process presents several advantages such as it is surfactant-free, easy to implement, and can accommodate several other polymer systems that are known to produce polymer aerogels. The balance of buoyancy and surface tension forces played significant role on droplet size and the number of inclusions within the droplet. Some preliminary results are presented in this work on thermal insulation behavior of multi-hollow polyimide aerogel particles. Such hollow areogel particles can be used in thermal insulation of small size objects, such as delicate sensors or in cleaning of noxious liquid spills in crevices.

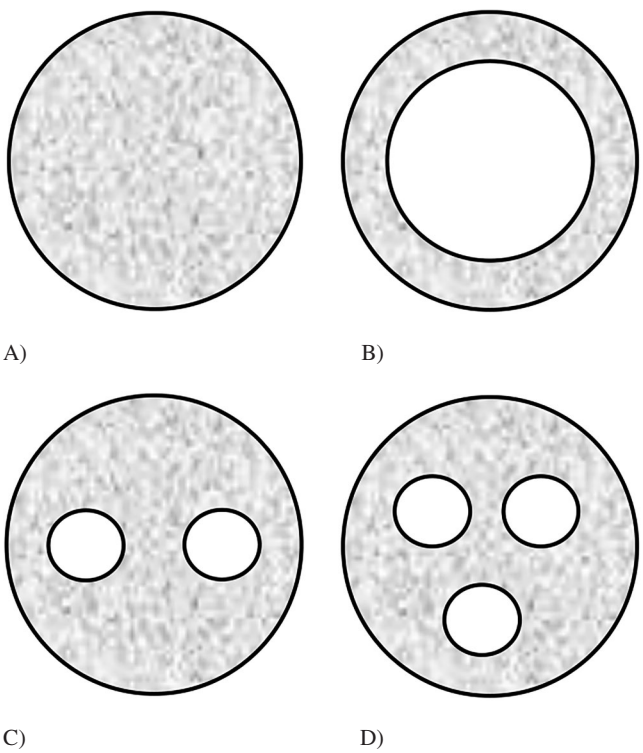


Fig. 1. Schematic representation of aerogel particles with internal, large size voids, A) no large size voids, B) core-shell particle, C) two internal voids, and (d) three internal voids

2 Experimental Section

2.1 Materials

Pyromellitic dianhydride (PMDA) was obtained from Alfa-Aesar (Haverhill, MA, USA) and 2,2′-dimethylbenzidine (DMBZ) was obtained from Shanghai Worldyang Chemical Co. Ltd. (Shanghai, PRC). Crosslinker molecule 1,3,5-benzenetricarbonyl trichloride (BTC), pyridine, and acetic anhydride were purchased from Sigma Aldrich (Milwaukee, WI, USA). Silicone oil with a room temperature density of 0.96 g/cm^3, acetone, and chloroform were purchased from Fisher Scientific (Ontario, NY, USA). N,N-dimethylformamide (DMF) with a room temperature density of 0.94 g/cm^3 was obtained from VWR International (Radnor, PA, USA). All reagents were directly used without purification. The components of the droplet generator including 0.16 cm ID Tee connectors, 27 G needle, PTFE tubing and Tygon tubing were purchased from McMaster-Carr (Aurora, OH, USA).

2.2 Preparation of Polyimide Sol

The polyimide chains were fabricated through the reaction Scheme shown in Fig. 2. The first reaction between the dianhydride (PMDA) and the diamine (DMBZ) formed the polyamic acid oligomers with the amine end groups, identified as compound (A) in Fig. 2. These oligomers were mixed with the dehydrating agent acetic anhydride and the accelerator pyridine to start the imidization reactions and obtain polyimide oligomer compound (B). The crosslinking of polyimide oligomers by BTC crosslinker was delayed to after imidization reactions to avoid reactions of BTC with the byproduct H_2O formed in the imidization step. The crosslinker addition led to three-dimensional polyimide networks, compound (C) and gelation.

The synthesis of polyimide sol at room temperature with 2.3 wt% solids concentration was based on 0.106 g DMBZ, 0.107 g PMDA, 0.018 g BTC, 0.33 ml acetic anhydride, 0.31 ml pyridine, and 9.0 ml DMF. First, PMDA was dissolved in 2 ml DMF under magnetic stirring at 1 000 min^{-1} for at least 30 min to ensure it was fully dissolved. Second, DMBZ was fully dissolved in 2 ml DMF under magnetic stirring at 1 000 min^{-1} for about 5 min. BTC was separately dissolved in 5 ml DMF under magnetic stirring at 1 000 min^{-1} for about 2 min. The polyamic acid was obtained by mixing the solutions of PMDA and DMBZ in DMF under magnetic stirring at 1 000 min^{-1} for 2 min. Afterwards, acetic anhydride and pyridine were added into the solution and stirred for 15 min to complete imidization of polyamic acid chains. The solution color changed to light yellow. BTC solution in DMF was then added to polyimide solution and stirred for another 2 min to obtain a polyimide sol.

IPP_IPP3989 – 10.9.20/reemers

2.3 Preparation of the Multi-Hollow Polyimide Aerogel Particles

A microfluidic droplet generator was used to convert polyimide sol into droplets inside the Tee-connector using a continuous medium of silicone oil, as shown in Fig. 3A-I. For this purpose, polyimide sol was carefully loaded in a 5 ml syringe pump. Separately, silicone oil was loaded in a 10 ml syringe pump. The flow rate (Q_d) of dispersed phase polyimide sol was fixed at 1.0 ml/min while the flow rate of silicone oil continuous phase (Q_c) was maintained at 0.1 ml/min all delivered at room temperature. It is noted that polyimide sol in DMF and silicone oil are immiscible. The dispersed and continuous phase liquids were guided into the Tee-connector through two 27 G needles (internal diameter 0.2 mm). The outlet stream from the Tee-connector was led through a Tygon tube into a hot silicone oil bath kept at 80 °C, as shown in Fig. 3B. The inner diameter of the Tee connector of the microfluidic device was 1.6 mm and that of Tygon delivery tube had inner and outer diameter respectively 1.6 mm and 3.2 mm.

The flow rate of the dispersed phase (polyimide sol) must be higher than the flow rate of the continuous phase (silicone oil) to obtain the dripping mode regime of microfluidic droplet generation, as shown in Fig. 3A-II. Due to the limited diameter of the Tygon tube and a factor of ten higher flow rate than silicone oil, the polyimide sol droplet generated by the dripping mode experienced elongation inside the Tygon tube and occupied much larger area than the intervening trains of silicone oil droplets shown in Fig. 3A-II. As shown in Fig. 3B, the train of silicone oil droplets floating in polyimide sol in the microfluidic channel were guided by Tygon delivery tube into the hot silicone oil bath kept at 80 °C. A polyimide sol droplet did not detach immediately at the exit of the Tygon tube due to an imbalance of the interfacial force that supported the droplet at the tube exit and the kinetic and buoyancy force that favored detachment. The droplet detached only sporadically once the sum of the kinetic and droplet buoyancy force outweighed the interfacial force. During this time-period, a plurality of silicone oil droplets entered the larger polyimide sol droplet. The detached polyimide sol droplet with embedded silicone oil droplets (Fig. 3B) entered the hot silicone

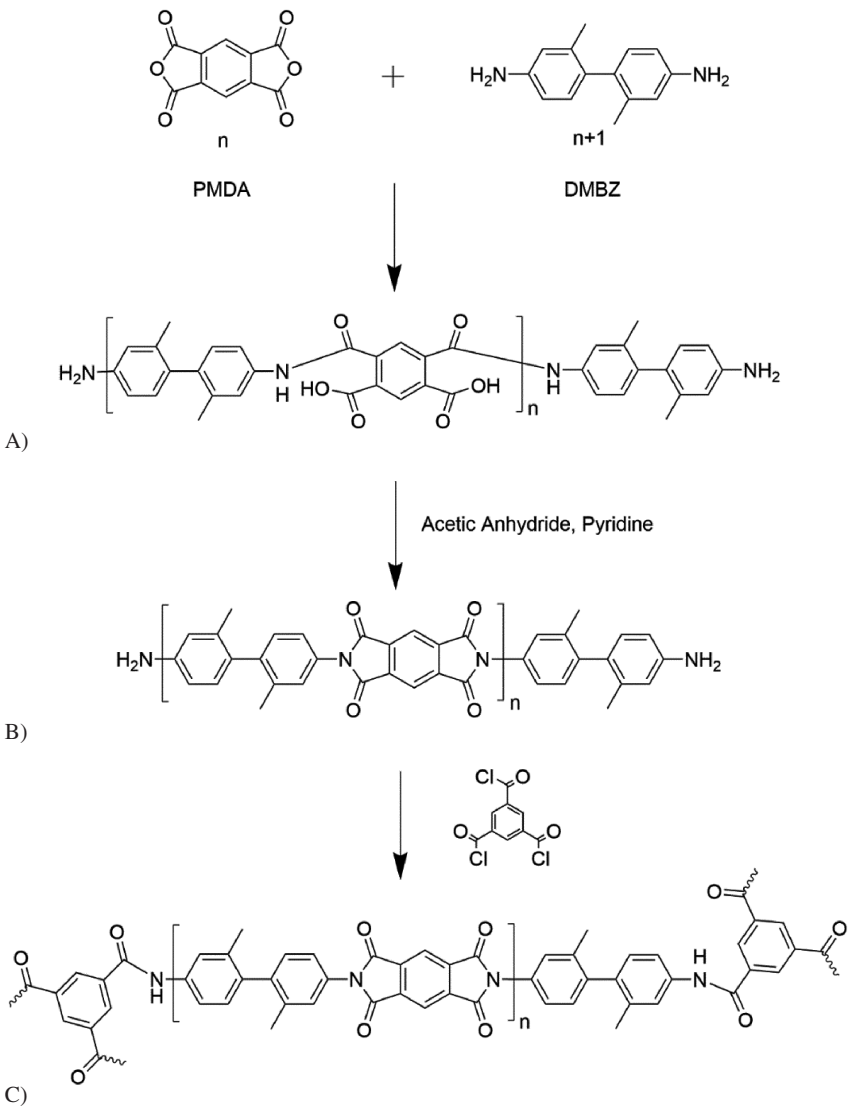
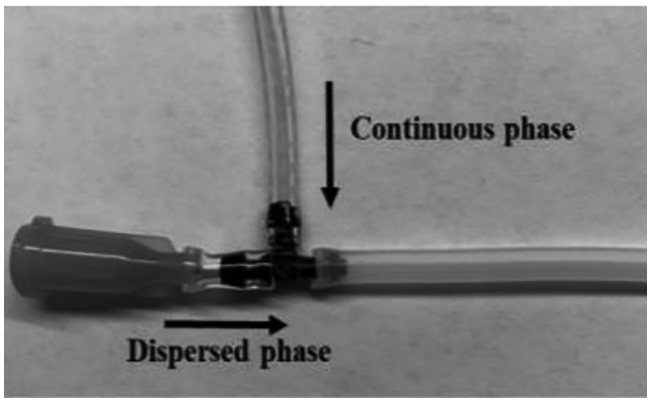
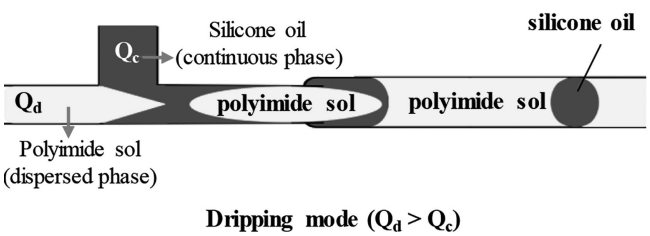


Fig. 2. Reaction scheme for synthesis of polyimide

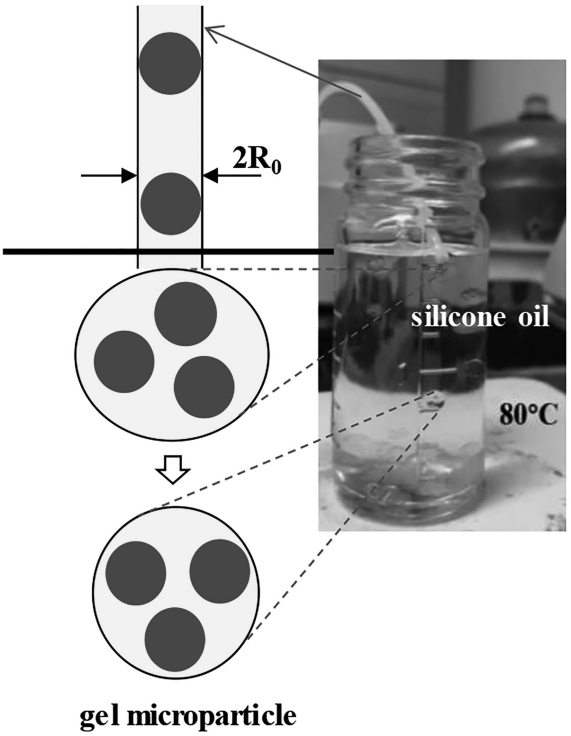
IPP_IPP3989 – 10.9.20/reemers



A-I)



A-II)



B)

Fig. 3. Schematic of formation of multi-hollow polyimide gel microparticles, A-I) T-junction of microfluidic droplet generator, A-II) polyimide sol microdroplet generation and flow through the tube, B) mechanism of inclusion of multiple silicone oil droplets in polyimide sol droplets inferred from images of actual experiments

oil bath and underwent gelation quickly, thus locking the internal silicone oil droplets in place.

The hot silicone oil expedited sol-gel transition of polyimide and consequently prevented coalescence of individual gel droplets. The process presented above can lead to polyimide sol droplets with multiple smaller silicone oil droplets included in them, depending on the balance of buoyancy force and the sum of kinetic force and interfacial force at the exit of the delivery tube. The illustration in Fig. 3B was inferred from an experimental video of the droplet formation process. It was noted that polyimide sol droplets did not easily break off at the end of the delivery tube under slow flow rate of polyimide sol. The interfacial force between silicone oil and polyimide sol supported the adjusted weight of polyimide sol droplets and prevented their detachment from the tip of the tube. In the meantime, a greater number of silicone oil droplets landed inside the hanging polyimide sol droplet. This eventually led to greater gravitational force and detachment of the droplet from the tube end. The hot silicone oil bath then expedited gelation of polyimide sol droplet and prevented coalescence of internal silicone oil droplets. The polyimide gel particles were collected at the bottom of the hot silicone oil bath.

The polyimide gel particles were collected, cooled down to room temperature in 24 h, and then gradually washed using chloroform to remove silicone oil from the gel. The washing step involved mixed solvents composed of 75 vol% chloroform/25 vol% acetone, 50 vol% chloroform/50 vol% acetone, 25 vol% chloroform/75 vol% acetone, and finally 100 vol% acetone. The gel particles were then washed five times in 100 vol% acetone at 24-hour intervals.

In conjunction, polyimide aerogel monoliths were fabricated following the same procedure described above. The polyimide sol was poured into a 13 mm diameter and 26 mm long cylindrical mold at room temperature and allowed to gel for 24 h followed by solvent exchange and supercritical drying.

The polyimide gel particles and cylindrical gel monoliths filled with acetone were subsequently transferred to an autoclave and exchanged with liquid carbon dioxide six times every 1.5 h. Finally, the autoclave was heated to 50 °C and under 11 MPa pressure which are above the critical temperature (31 °C) and pressure (7.38 MPa) of carbon dioxide to convert gel into aerogel.

2.4 Characterization of Multi-Hollow Polyimide Aerogel Particles

2.4.1 Microscopy

The morphology of aerogel particles was observed through a scanning electron microscope (SEM, model JSM5310, Jeol, ■■Peabody■■, MA, USA) at an accelerating voltage of 5 kV and emission current of 20 mA. A representative aerogel parti-cle and a piece of fractured aerogel particle specimen were mounted on an aluminum stub using carbon tape, followed by sputter coating with silver (model ISI-5400 Sputter Coater, Polaron, ■■Laughton■■, UK). The morphology of gel and aero-gel particles were studied using an optical microscope (OM, model BX51, Olympus, ■■Center Valley, USA■■).

2.4.2 Surface Tension Measurements

The surface tension of DMF and the interfacial tension between DMF and silicone oil were measured at room temperature using a force tensiometer (model K20, KRÜSS Scientific Instruments, Inc., ■■Matthews■■ NC, USA)

2.4.3 IR and NMR Spectroscopy

Infrared spectra were obtained on a FTIR tri-detector spectrophotometer (model Nicolet iS20, Thermo Scientific, ■■Waltham■■, MA, USA). ^{13}C NMR cross-polarization and CP-TOSS NMR spectra were collected on a 500 MHz (11.7
T) spectrometer (model Varian NMRS, ■■Varian Inc, Palo Alto, CA,USA■■) operated at 125.62 MHz for ^{13}C and equipped with a narrow-bore triple-resonance T3 MAS NMR probe (also Varian). Samples were packed into 4 mm zirconia rotors and spun about the magic angle at 12 kHz. Cross-polarization ex-periments were collected with a 50 kHz spectral window, a 0.04 s acquisition time, a 5 s relaxation delay, 1,024 scans, 62.5 kHz cross-polarization and SPINAL decoupling fields, and a 5 ms cross-polarization period using a linear-ramped cross-polarization method. The methyl peak of hexamethyl-benzene at 17.3 ppm was used as a secondary chemical shift reference.

2.4.4 Thermogravimetry

Thermogravimetric analysis (TGA) was conducted under N_2 environment with a thermogravimetric analyzer (model TA Q500, TA Instruments, ■■New Castle■■, DE, USA) using a heating rate of 10 °C/min, from 25 °C up to 800 °C.

2.4.5 Pore Volume and Porosity

Porosity was calculated from the bulk density (ρ_b) and skeletal (ρ_s) according to Eq. 1. The bulk density was calculated from the volume and mass of the aerogel monolith. The data on skeletal density was obtained through a helium pycnometer (model AccuPyc II 1340, Micromeritics Instrument Corp., ■■Norcross■■, GA, USA). The helium pycnometer was cali-brated for each measurement.

$$\text{porosity} = \left(1 - \frac{\rho_b}{\rho_s}\right) \times 100\%. \quad (1)$$

Note that only the bulk density of aerogel monoliths synthesized under identical condition was obtained. It was difficult to isolate individual particles for measurement of weight and diameter.

2.4.6 Brunauer-Emmett-Teller (BET) Surface Area

BET surface area and pore size distribution of both multi-hollow polyimide aerogel particles and non-hollow polyimide aerogel particles were obtained from N_2 adsorption-desorption isotherms at 77 K, using a Tristar II 3020 analyzer (Micromeritics Instrument Corp.). The pore size distribution was obtained from isotherms following the Barrett-Joyner-Halenda (BJH) model.

2.4.7 Gel Time and Viscosity

The crossover point of the storage (G′) and loss (G″) moduli provided the gel time for polyimide solution at room temperature (24 °C). For this purpose, the rheometer (model DHR-2, TA Instruments, New Castle, DE, USA) was used in shear mode. The reaction mixture was loaded into the rheometer fitted with a 25 mm parallel plate set up. The rheometer was operated at a constant angular frequency of 1 rad/s at 10 % strain. The gelation time was obtained by adding the elapsed time in preparation of the sol and the time obtained from rheometry.

2.4.8 Thermal Performance

A representative set of multi-hollow polyimide aerogel particles was placed on a heated metal plate and the temperature of the plate was raised from room temperature first to 70 °C and then to 100 °C. A blank experiment without the particles confirmed uniform temperature of the metal plate within ±2 °C. Test particles were placed close to each other and thus were subjected to uniform plate temperature. The temperature was held at 100 °C for 10 mins. A camera (model 225 IR, Fotric Thermal Imaging Technology Company, Dallas, TX, USA) was used to capture the temperature difference between the multi-hollow polyimide aerogel particles and the heated metal plate. The camera spatial resolution was 1.27 mrad and the temperature resolution was ±2 °C. The non-hollow polyimide aerogel microparticles were also heated to compare the data with the hollow particles.

3 Results and Discussions

This section first examines the morphology of aerogel particles. It was indicated in the experimental section that the internal diameter of Tygon tube was 1.6 mm and the flow rate of polyimide sol was a factor of ten higher than that of silicone oil. Accordingly, the droplets of polyimide sol generated in the Tee-connector under dripping mode (Clanet and Lasheras, 1999) were large and covered the entire tube as cylindrical threads with intervening silicone oil droplets, as shown in Fig. 3A-II and 3B. In view of the above, the polyimide gel particles produced in this work had diameter of the order of a millimeter, as opposed to a few hundred micrometer obtained using jetting mode as reported by Teo and Jana (2019). In this context, we first discuss why the ratio of Q_d and Q_c was maintained at 10.0.

3.1 Role of the Ratio of Q_d and Q_c on Droplet Generation

It was presented in the Experimental section that a dripping regime (Clanet and Lasheras, 1999) of droplet generation was

IPP_IPP3989 – 10.9.20/reemers

used to produce multi-hollow polyimide aerogel particles. The dripping regime was achieved in this work by maintaining the values of Q_c and Q_d at respectively 0.1 and 1.0 ml/min. A rationale is now presented for selecting the above flow rates. We conducted a series of experiments to obtain an appropriate condition for the dripping regime, as multi-hollow gel and aerogel particles could be obtained only in this regime. For this purpose, the droplet generation process was studied using blue colored DMF as the dispersed liquid instead of polyimide sol and by varying the values of Q_c for a given value of Q_d = 1.0 ml/min, in the following combinations – (a) $Q_c > Q_d$ with Q_c = 2.0 ml/min; (b) $Q_c < Q_d$, with Q_c = 0.9 ml/min, and (c) $Q_c < Q_d$ with Q_c = 0.1 ml/min. The DMF phase was colored by dissolving methylene blue to enable tracking of the motion of droplets. It is noted that methylene blue is not soluble in silicone oil.

A set of snapshots were taken of the Tygon delivery tube showing the domains of colored DMF and clear silicone oil inside the tube, as shown in Fig. 4. It is apparent from the images that jetting regime (Fig. 4A) would not produce multi-hollow gel particles. This regime was used by Teo and Jana (2019) to produce aerogel microparticles of a few hundreds of micrometer diameter. Figure 4B and C both represent the dripping regime. However, the multi-hollow aerogel particles were obtained only for the conditions of Fig. 4C. In view of this, the materials presented and discussed in the rest of paper were produced with Q_c and Q_d of respectively 0.1 and 1.0 ml/min.

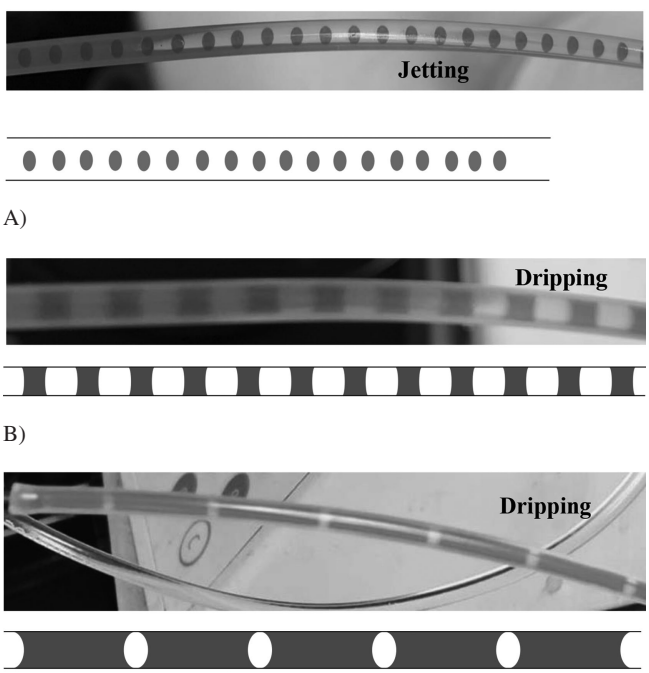


Fig. 4. Effects of flow rates, Q_c and Q_d, on drop formation regime. Trains of domains/droplets of DMF (blue) and silicone oil (white) are presented, A) jetting regim with Q_c = 2.0 ml/min, B) dripping regime with Q_c = 0.9 ml/min, C) dripping regime Q_c = 0.1 ml/min all with Q_d = 1.0 ml/min

3.2 Gel and Aerogel Particle Size Distributions

The distribution of diameter of gel and aerogel particles are presented in Fig. 5A. It is apparent that the gel particles had diameter in the range of 1 500 to 1 775 μm, with the most probable gel particle diameter of 1 675 μm. The aerogel particle diameter shifted to smaller values, e. g., to the range of 1 450 to 1 680 μm, due to volume shrinkage in the supercritical drying step. The above distributions were generated by reading the diameter of more than 100 gel and aerogel particles. It is noted that each gel and aerogel particles contained five (5) internal voids. In conjunction, the diameter of each internal void was also measured and a distribution was generated from at least 100 data points, as shown in Fig. 5B. The mean diameter of gel particles was 1 647 ± 65 μm with corresponding mean internal void diameter of 432 ± 14 μm. The supercritically dried polyimide aerogel particles had mean di-

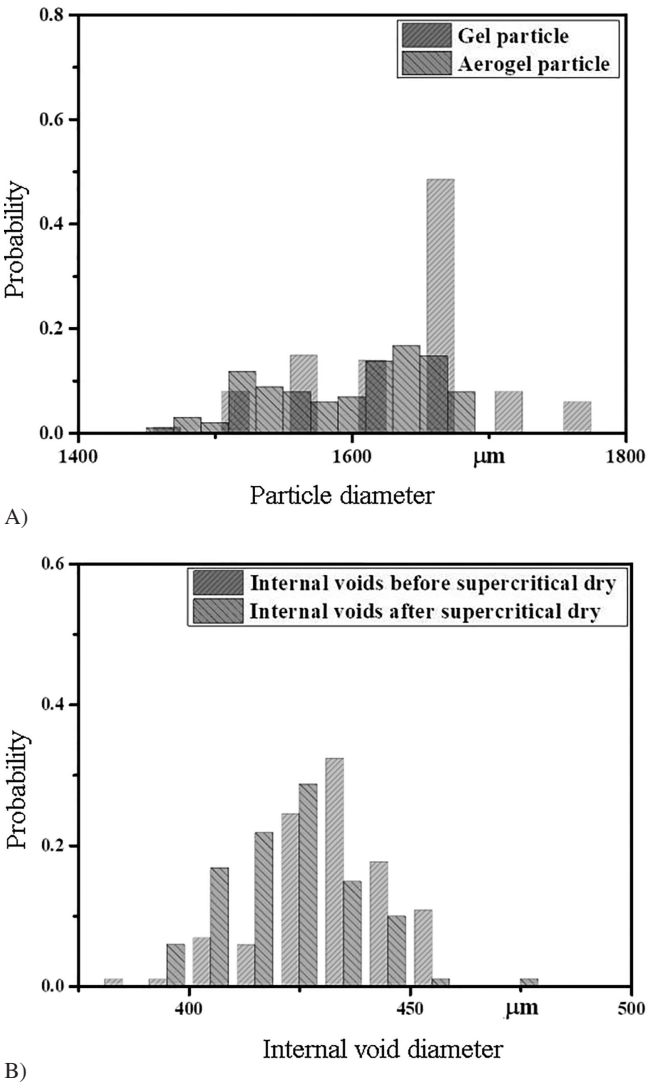


Fig. 5. Diameter distribution of gel and aerogel particles (A), distribution of internal void diameter in gel and aerogel particles (B). Each gel and aerogel particles contained five (5) internal voids

IPP_IPP3989 – 10.9.20/reemers

ameter of 1 589 ± 58 µm and corresponding internal void diameter of 422 ± 15 µm. In each case, a standard deviation of particle diameter was computed from the diameter of more than 100 particles inferred from ImageJ software (■■National Institute of Health, Bethesda, MD, USA■■).

3.3 The Morphology of Multi-Hollow Polyimide Aerogel Particles

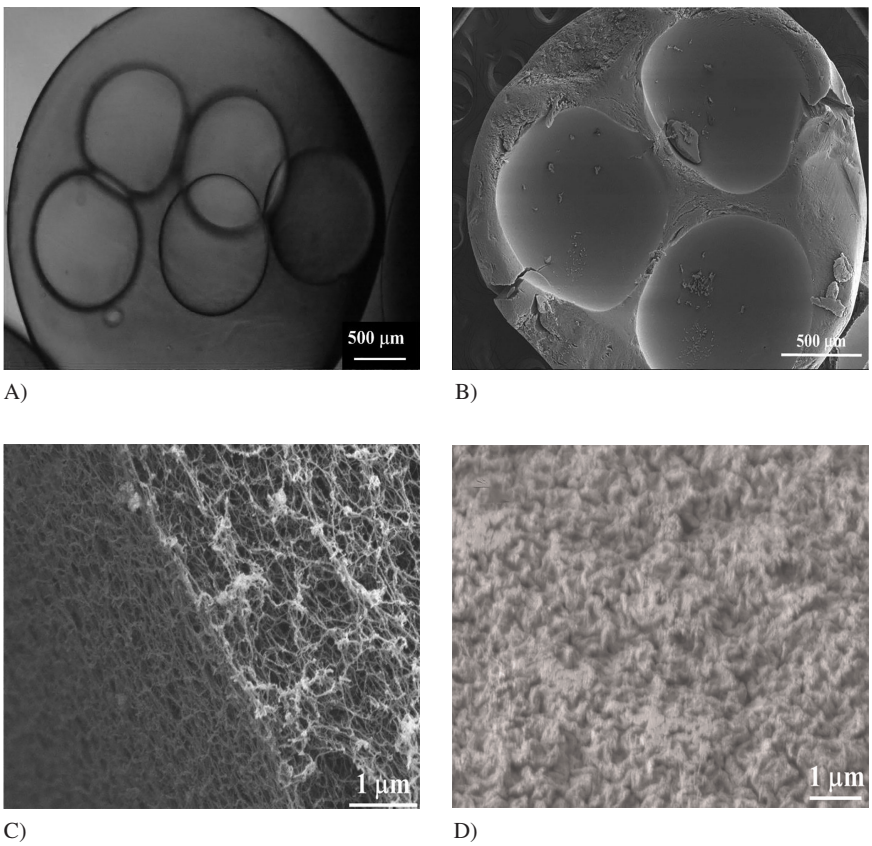
An optical image of a representative nearly spherical polyimide aerogel particle in Fig. 6A shows five internal voids originating from silicone oil droplets. In view of the scale bar presented in Fig. 6A, the internal voids had a diameter of approximately 500 µm and the multi-hollow aerogel particle had a diameter of about 2.0 mm. The image in Fig. 6A also indicates that silicone oil droplets did not undergo coalescence inside the polyimide sol droplets.

The SEM image of a fractured aerogel particle presented in Fig. 6B shows three internal voids of diameter close to 500 µm, placed symmetrically in the cross-section and separated by the skin layers with the thinnest part of thickness approximately 50 µm. A higher magnification SEM image in Fig. 6C shows the porous nature of the skin between the neighboring voids and the porous nature of the interface between silicone oil and polyimide sol in the gel droplet, as was observed in the case of emulsion-templated aerogel foams (Teo and Jana, 2017; Teo et al., 2018; Mawhinney and Jana, 2019) and core-shell aerogel microparticles (Teo et al., 2020). The surface of the aerogel particles was also found porous as revealed from the SEM image presented in Fig. 6D. The solvent exchange using chloroform and acetone mixture and supercritical drying were possible due to the porous nature of the gel particles.

A close examination of the morphology of the void surface in Fig. 6C and the aerogel particle surface in Fig. 6D indicate the presence of wrinkles on the external surface of the aerogel particles. This was earlier observed by Teo and Jana (2019) and attributed to higher degree of molecular diffusion between DMF and silicone oil at silicone bath temperature of 80 °C.

3.4 The Time Window for Droplet Generation

A simple tracking of the time elapsed in loading of polyimide sol and silicone oil in the syringe pumps revealed that polyimide microparticles were generated within 19 min of mixing of the polyimide precursors into polyimide sol. In this context, it is important to note if substantial gelation of polyimide sol would occur in this time-period. The rheology data presented in Fig. 7A show the crossover point of the loss (G'') and the storage modulus (G') values, thus yielding a sol-gel transition time of the polyimide system ∼ 34 mins. The complex viscosity data in Fig. 7B show that the viscosity of the polyimide sol remained almost constant before the sol-gel transition. This suggests that the viscosity ratio of the dispersed and continuous



A) B) C) D)

Fig. 6. Representative images of aerogel particle, A) optical microscope of the multi-hollow polyimide aerogel particle, B) SEM image of deliberately fractured aerogel particle, C) hollow nature of aerogel particle, D) morphology of the outer surface of aerogel particle

IPP_IPP3989 – 10.9.20/reemers

phases did not change during generation of polyimide droplets. According to Teo and Jana (2019), the heated silicone oil bath at 80 °C would speed up the sol-gel transition reactions to about 10 s. This confirms that the sol droplets turned into gel particles within 10 s of arrival into hot silicone oil bath and thus coalescence was not a concern in this work.

3.5 Analysis of Polyimide Droplet Formation with Multiple Internal Droplet Inclusions

We now present an analysis of polyimide sol droplet formation, especially the ones that contained multiple internal droplets of silicone oil. Teo and Jana (2019) reported silicone oil viscosity of ~48.6 mPa s at room temperature. The interfacial tension (Γ) between DMF and silicone oil was measured at room temperature to be 4.2 mN/m. Teo and Jana (2019) reported a value of 3.0 mN/m. The viscosity of the polyimide sol was determined to be 0.5 Pa s at room temperature, as per Fig. 7B. The density of silicone oil and DMF at room temperatures were respectively 0.96 and 0.94 g/cm^3. Considering 2.3 wt% polyimide in the sol, the sol density (ρ_{sol}) at room temperature was calculated to be 0.961 g/cm^3, while the density of silicone oil (ρ_{sil}) in the bath at 80 °C was 0.916 g/cm^3. In view of Fig. 3B, a polyimide sol droplet of radius R_1 can hang from the inside tip of the Tygon tube of radius R_0 from a balance of the interfacial force, F_{int} and the buoyancy F_b as in Eq. 2:

$$F_{int} = F_b, \tag{2}$$

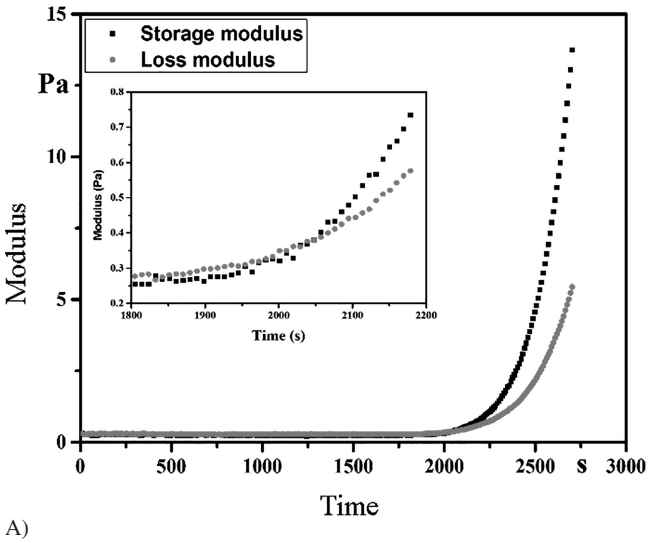
where, the expressions of F_{int} and F_b are given in Eq. 3 and 4 respectively.

$$F_{int} = 2\pi R_0 \Gamma, \tag{3}$$

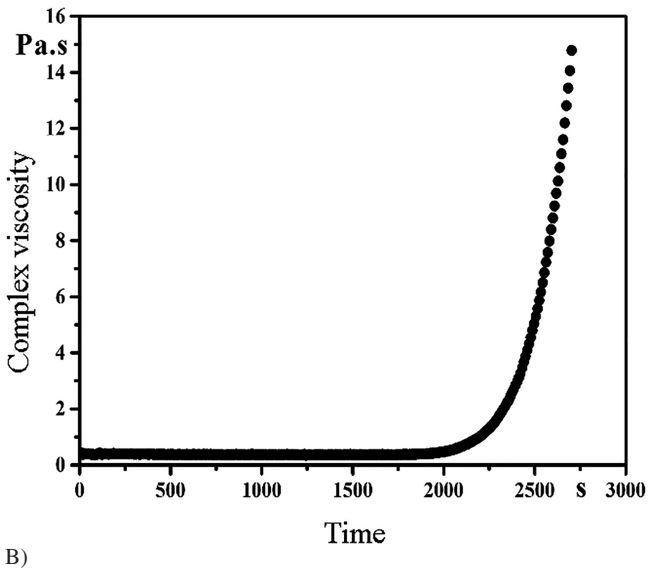
$$F_b = 4/3\pi {R_1}^3(\rho_{sol} - \rho_{sil})g. \tag{4}$$

In Eq. 3, Γ is the interfacial tension, and in Eq. 4, g is the gravitational acceleration. The kinetic force contribution can be neglected in view of small value of Reynolds number ~0.0025 calculated based on Tygon tube diameter of 1.6 mm, Q_d of 1.0 ml/min that yields an average velocity of 0.833 mm/s through the Tygon tube, and polyimide sol viscosity of 0.5 Pa s as inferred from the data in Fig. 7B.

The balance of interfacial force and buoyancy force yields an equilibrium value of R_1 to be 2.25 mm, indicating that sol droplets need to grow to beyond a radius of 2.25 mm before the buoyancy force can detach the droplet from the tip of the tube. This value compares well with the size of polyimide aerogel particle of 2.0 mm reported in Fig. 6A. At polyimide sol flow rate of 1.0 ml/min in this work, this takes about 0.7 s for each droplet to form. In the meantime, silicone oil droplets keep entering the polyimide sol droplet and make up for about 1/10th the droplet volume before droplet detachment occurs.



A)



B)

Fig. 7. Storage modulus and loss modulus traces of the polyimide sol (A), complex viscosity vs. time curve of the polyimide sol (B)

3.6 Monitoring of Imidization and Thermal Properties

The knowledge of imidization and thermal stability of polyimide aerogel particles was gleaned from IR and NMR spectroscopy data and thermogravimetric analysis as presented in Fig. 8. The IR spectra in Fig. 8A correspond to the multi-hollow polyimide aerogel particles. The lack of sharp peak at 3 000 cm^{-1} and 1 620 cm^{-1} showed that the end amine groups in polyamic acid were reacted and converted into the imide functional group. The strong peaks at 724, 1 100, 1 370, 1 717, 1 779 cm^{-1} represented the presence of the imide functional groups. The peak at 724 cm^{-1} indicated the bending of C=O group, whereas the peaks at 1 717, 1 779 cm^{-1} corresponded to the asymmetric and symmetrical carbonyl stretching. The peak at 1 370 cm^{-1} represented the stretching of C-N group, while the absorbance peak at 1 100 cm^{-1} was attributed to the deformation of the imide rings. The solid-state NMR spectra of the multi-hollow polyimide aerogel materials are shown in Fig. 8B. The sharp peak at 165.4 ppm indicates the presence of imide carbonyl group, whereas the peaks at 137.8, 131.0, 117.4 ppm represent the aromatic carbons.

IPP_IPP3989 – 10.9.20/reemers

The TGA trace in Fig. 8C reveals only 10 % weight loss of the multi-hollow polyimide aerogel particle at about 550 °C indicating that the imidization of the polyimide had gone to nearly completion at room temperature.

3.7 Surface Area and Porosity

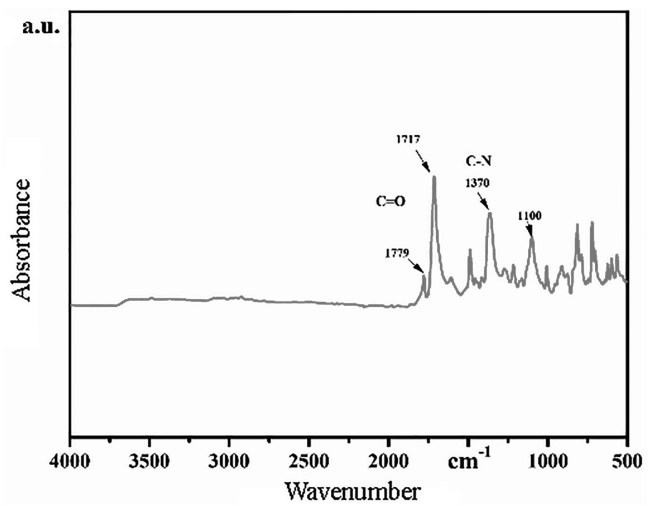
The nitrogen adsorption-desorption diagrams of multi-hollow aerogel particles and aerogel monoliths are presented in Fig. 9. The hysteresis between adsorption and desorption curves at P/P_0 ratio of 0.8 in Fig. 9A, C indicate that the materials followed Type IV adsorption-desorption isotherms and contained mesopores. The specific BET surface area of multi-hollow polyimide aerogel particles and monoliths were respectively 481 and 347 m^2/g. Recall that polyimide aerogel monolith was produced by completing sol-gel transition at room temperature. Accordingly, the system took about 34 min to obtain the gel as per Fig. 7A. The gel was then aged for 24 h. In comparison, the polyimide sol droplets turned into multi-hollow gel particles much more rapidly, in about 10 s after reaching the hot silicone oil kept at 80 °C. Accordingly, the polyimide strands that formed the gel networks in multi-hollow gel particles were thinner due to rapid liquid-solid phase separation. These thinner strands produced higher specific surface area in multi-hollow aerogel particles.

The pore size distributions obtained from Barrett-Joyner-Halenda method are presented in Fig. 9B, D. It is evident that the most probable mesopore diameter in both cases was ~40 nm, although the aerogel monolith had narrower pore size distribution. As alluded to earlier, gelation in the case of multi-hollow gel particle occurred under a thermal gradient. The sol droplet contacted silicone oil at 80 °C. The diffusive heat transport from hot silicone oil into the sol droplet also caused a gradient of the speed of gelation and accordingly caused different pore structures.

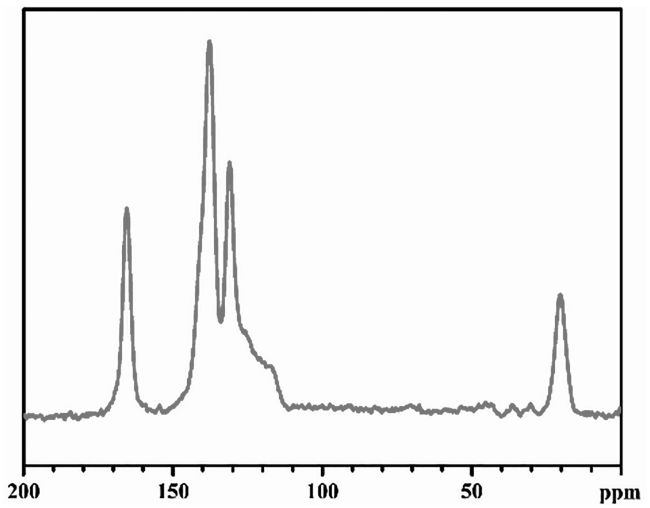
3.8 Thermal Insulation

The temperature of two aerogel particles – one multi-hollow and one non-hollow – was monitored over time, after a metal plate on which the particles were stationed was heated from room temperature first to 70 °C and then to 100 °C. An infrared thermal camera was used to register the temperature of the metal plate, the domains around the aerogel particles, and the aerogel particles. A lower temperature of the aerogel particles than the metal plate presented evidence that aerogel particles were thermally insulating. However, it was not known a priori if the non-hollow or the multi-hollow aerogel particle would provide better thermal insulation. We recall from Fig. 9 that both these particles contained substantial mesopores.

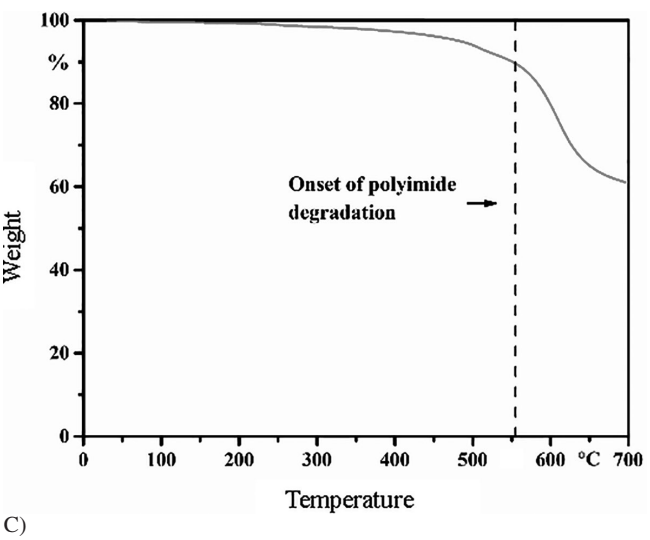
The thermal scan image data presented in Fig. 10A show the initial thermal condition of the metal plate and the aerogel particles, the latter identified with arrows. Figure 10B shows the equilibrium thermal image when the plate was heated to 70 °C. It is apparent from the black curve in Fig. 10E that the temperature of the particles were lower than that of the plate, thus showing good thermal insulation behavior of the polyi-



A)



B)



C)

Fig. 8. IR spectra (A), solid ^{13}C NMR (B) and TGA curve (C) of multi-hollow polyimide aerogel particles

IPP_IPP3989 – 10.9.20/reemers

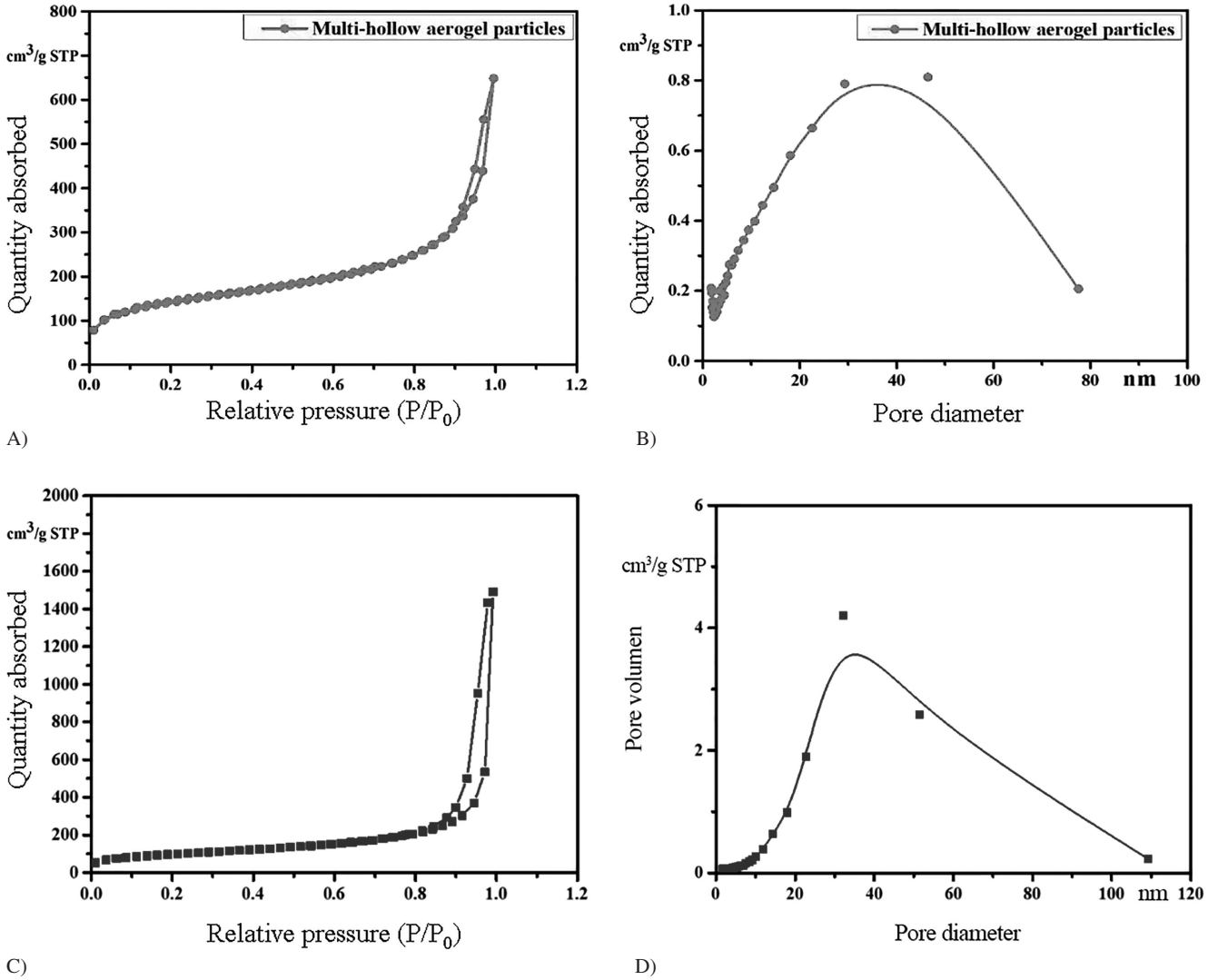


Fig. 9. BET isotherms (A, C) and pore volume vs pore diameter curves (B, D) of multi-hollow polyimide aerogel particles (A, B) and polyimide

mide aerogel particles attributed to the Knudsen effect (Notario et al., 2015; Zhao et al., 2012). Judging by the closeness of the depth of the well of temperature profile, both multi-hollow and non-hollow particles had the same temperature. Figure 10C and D shows respectively the thermal image of the plate and the aerogel particles while in the process of heating to the set temperature of 100 °C and at equilibrium at 100 °C. The corresponding aerogel temperature profiles represented respectively by the red and the blue curves in Fig. 10E now indicate recognizable difference of temperature of the articles – the multi-hollow aerogel particle had about 5 °C lower temperature than the non-hollow particle. The presence of higher quantity of macro-pores in multi-hollow aerogel particles offered greater resistance to thermal transport (Hou et al., 2019).

4 Conclusion

This work presented an easier method to obtain surfactant-free multi-hollow polyimide aerogel particles using a one-step set-up of the microfluidic device. The dripping regime and the flow rates adopted in this work consistently produced aerogel particles with five internal voids. The data presented in this work established the parameters of a microfluidic flow device that can be used for fabrication of an array of aerogel particles with one or plurality of internal voids by tuning the flow rates of the two streams. The multi-hollow polyimide aerogel particles presented higher BET surface area than monoliths and better performance in thermal insulation compared to the non-hollow polyimide aerogel particles.

IPP_IPP3989 – 10.9.20/reemers

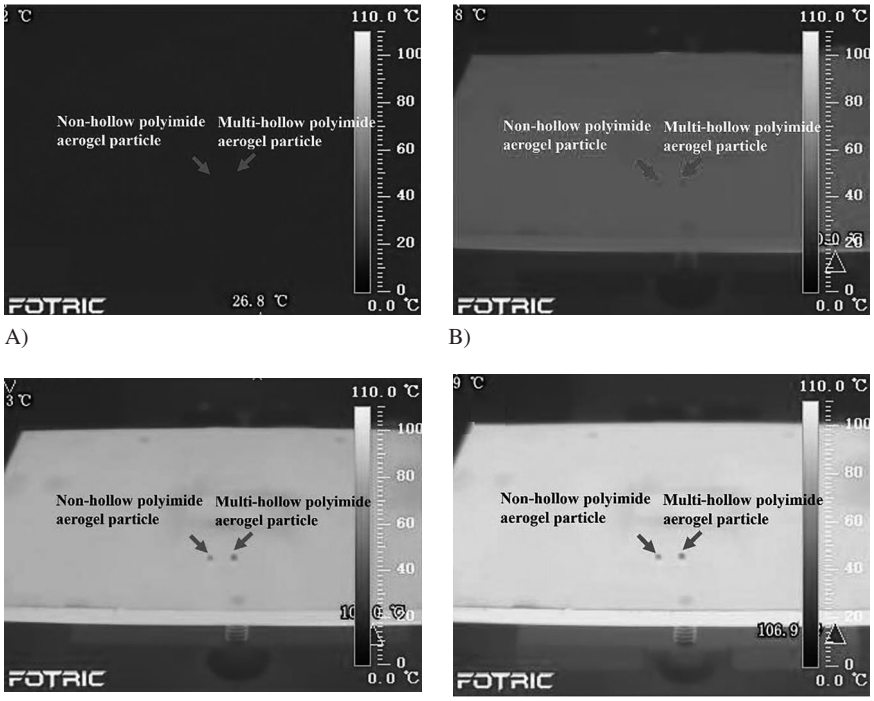


Fig. 10. Heating of representative non-hollow and multi-hollow (5 internal voids) aerogel particles are identified by arrows stationed on the metal plate, A) IR camera image at room temperature, B) IR camera image when the heat plate was set to 70°C, C) IR camera image when the heat plate was set to 100°C, D) IR camera image when the heat plate was kept at 100°C for 10 mins, and (E) temperature traces of aerogel particles at different set temperatures

References

Alnaief, M., Smirnova, I., "Effect of Surface Functionalization of Silica Aerogel on Their Adsorptive and Release Properties", J. Non-Cryst. Solids, **356**, 1644–1649 (2010), DOI:10.1016/j.jnoncrysol.2010.06.027

Alnaief, M., Smirnova, I., "In situ Production of Spherical Aerogel Microparticles", J. Supercrit. Fluids, **55**, 1118–1123 (2011), DOI:10.1016/j.supflu.2010.10.006

Chen, H., Zhao, Y., Song, Y. and Jiang, L., "One-Step Multicomponent Encapsulation by Compound-Fluidic Electrospray", J. Am. Chem. Soc., **130**, 7800–7801 (2008), PMid:18510318; DOI:10.1021/ja801803x

Clanet, C., Lasheras, J. C., "Transition from Dripping to Jetting", J. Fluid Mech., **383**, 307–326 (1999), DOI:10.1017/S0022112098004066

Dendukuri, D., Doyle, P. S., "The Synthesis and Assembly of Polymeric Microparticles Using Microfluidics", Adv. Mater., **21**, 4071–4086 (2009), DOI:10.1002/adma.200803386

Edwards, W. M., Maxwell, R. I. U. S. Patent 2 710 853 A (1955)

Gu, S., Zhai, C. and Jana, S. C., "Aerogel Microparticles from Oil-In-Oil Emulsion Systems", Langmuir, **32**, 5637–5645 (2016), PMid:27183146; DOI:10.1021/acs.langmuir.6b01043

Guo, H., Meador, M. A. B., Mccorkle, L., Quade, D. J., Guo, J., Hamilton, B., Cakmak, M. and Sprowl, G., "Polyimide Aerogels Cross-Linked through Amine Functionalized Polyoligomeric Silsesquioxane", ACS Appl. Mater. Interfaces, **3**, 546–552 (2011), PMid:21294517; DOI:10.1021/am101123h

Guo, H., Meador, M. A. B., Mccorkle, L., Quade, D. J., Guo, J., Hamilton, B. and Cakmak, M., "Tailoring Properties of Cross-Linked Polyimide Aerogels for Better Moisture Resistance, Flexibility,

IPP_IPP3989 – 10.9.20/reemers

and Strength", ACS Appl. Mater. Interfaces, **4**, 5422–5429 (2012), PMid:22956659; DOI:10.1021/am301347a
Hou, D., Li, T., Chen, X., He, S., Dai, J., Mofid, S. A., Hou, D., Iddya, A., Jassby, D., Yang, R., Hu, L. and Ren, Z. J., "Hydrophobic Nanostructured Wood Membrane for Thermally Efficient Distillation", ■■Science Advances■■, **5**, ■■Eaaw3203(1-9)■■ (2019), PMid:31414047; DOI:10.1126/sciadv.aaw3203
Jones, S. M., "Aerogel: Space Exploration Applications", Journal of Sol-Gel Science and Technology, **40**, 351–357 (2006), DOI:10.1007/s10971-006-7762-7
Kim, J., Kwon, J., Kim, S.-I., Kim, M., Lee, D., Lee, S., Kim, G., Lee, J. and Han, H., "One-Step Synthesis of Nano-Porous Monolithic Polyimide Aerogel", Microporous Mesoporous Mater., **234**, 35–42 (2016), DOI:10.1016/j.micromeso.2016.06.037
Kwon, J., Kim, J., Yoo, T., Park, D. and Han, H., "Preparation and Characterization of Spherical Polyimide Aerogel Microparticles", Macromol. Mater. Eng., **299**, 1081–1088 (2014), DOI:10.1002/mame.201400010
Marquis, M., Davy, J., Cathala, B., Fang, A. and Renard, D., "Microfluidics Assisted Generation of Innovative Polysaccharide Hydrogel Microparticles", Carbohydr. Polym., **116**, 189–199 (2015), PMid:25458289; DOI:10.1016/j.carbpol.2014.01.083
Mawhinney, K., Jana, S. C., "Design of Emulsion-Templated Mesoporous-Macroporous Polyurea Gels and Aerogels", ACS Appl. Polym. Mater., **1**, 3115–3129 (2019), DOI:10.1021/acsapm.9b00762
Meador, M. A. B., Alemán, C. R., Hanson, K., Ramirez, N., Vivod, S. L., Wilmoth, N. and Mccorkle, L., "Polyimide Aerogels with Amide Cross-Links: A Low Cost Alternative for Mechanically Strong Polymer Aerogels", ACS Appl. Mater. Interfaces, **7**, 1240–1249 (2015), PMid:25564878; DOI:10.1021/am507268c
Meador, M. A. B., Malow, E. J., Silva, R., Wright, S., Quade, D., Vivod, S. L., Guo, H., Guo, J. and Cakmak, M., "Mechanically Strong, Flexible Polyimide Aerogels Cross-Linked with Aromatic Triamine", ACS Appl. Mater. Interfaces, **4**, 536–544 (2012), PMid:22233638; DOI:10.1021/am2014635
Nguyen, B. N., Meador, M. A. B., Scheiman, D. and Mccorkle, L., "Polyimide Aerogels Using Triisocyanate as Cross-Linker", ACS Appl. Mater. Interfaces, **9**, 27313–27321 (2017), PMid:28737037; DOI:10.1021/acsami.7b07821
Notario, B., Pinto, J., Solorzano, E., De Saja, J. A., Dumon, M. and Rodríguez-Pérez, M. A., "Experimental Validation of the Knudsen Effect in Nanocellular Polymeric Foams", Polymer, **56**, 57–67 (2015), DOI:10.1016/j.polymer.2014.10.006
Okushima, S., Nisisako, T., Torii, T. and Higuchi, T., "Controlled Production of Monodisperse Double Emulsions by Two-Step Droplet Breakup in Microfluidic Devices", Langmuir, **20**, 9905–9908 (2004), PMid:15518471; DOI:10.1021/la0480336
Saadatnia, Z., Mosanenzadeh, S. G., Esmailzadeh, E. and Naguib, H. E., "A High Performance Triboelectric Nanogenerator Using Porous Polyimide Aerogel Film", Scientific Reports, **9**, 1370–■■? (2019), PMid:30718775; DOI:10.1038/s41598-018-38121-1
Sabri, F., Marchetta, J., and Smith, K. M., "Thermal Conductivity Studies of a Polyurea Cross-Linked Silica Aerogel-RTV 655 Compound for Cryogenic Propellant Tank Applications in Space", Acta Astronaut., **91**, 173–179 (2013), DOI:10.1016/j.actaastro.2013.06.001
Teo, N., Jana, S. C., "Surfactant-Free Process for the Fabrication of Polyimide Aerogel Microparticles", Langmuir, **35**, 2303–2312 (2019), PMid:30650304; DOI:10.1021/acs.langmuir.8b03841
Teo, N., Gu, Z. and Jana, S. C. "Polyimide-Based Aerogel Foams via Emulsion-Templating", Polymer, **157**, 95–102 (2018), DOI:10.1016/j.polymer.2018.10.030
Teo, N., Jana, S. C., "Solvent Effects on Tuning Pore Structures in Polyimide Aerogels", Langmuir, **34**, 8581–8590 (2018), PMid:29957959; DOI:10.1021/acs.langmuir.8b01513
Teo, N., Jana, S.C., "Open Cell Aerogel Foams via Emulsion Templating". Langmuir, **33**, 12729–12738 (2017), PMid:29048907; DOI:10.1021/acs.langmuir.7b03139
Teo, N., Jin, C., Kulkarni, A. and Jana, S. C., "Continuous Fabrication of Core-Shell Aerogel Microparticles Using Microfluidic Flows", J. Colloid Interface Sci., **561**, 772–781 (2020), PMid:31761464; DOI:10.1016/j.jcis.2019.11.053
Teo, N., Joo, P., Amis, E. J. and Jana, S. C., "Development of Intricate Aerogel Articles Using Fused Filament Fabrication", ACS Appl. Polym. Mater., **1**, 1749–1756 (2019), DOI:10.1021/acsapm.9b00301
Wang, W., Zhang, M.-J., and Chu, L.-Y., "Functional Polymeric Microparticles Engineered from Controllable Microfluidic Emulsions", Acc. Chem. Res., **47**, 373–384 (2014), PMid:24199893; DOI:10.1021/ar4001263
Zhao, J.-J., Duan, Y.-Y, Wang, X.-D. and Wang, B.-X., "Effects of Solid–Gas Coupling and Pore and Particle Microstructures on the Effective Gaseous Thermal Conductivity in Aerogels", J. Nanopart. Res., **14**, 1024 (2012), DOI:10.1007/s11051-012-1024-0

Acknowledgements

This work is partially funded by National Science Foundation under grant number CMMI 1826030.

Date received: May 24, 2020
Date accepted: July 18, 2020

Bibliography
DOI 10.3139/217.3989
Intern. Polymer Processing
XXXV (2020) 5; page 1–12
© Carl Hanser Verlag GmbH & Co. KG
ISSN 0930-777X